CARBON

Mechanical and structural characterization of electrospun PAN-derived carbon nanofibers

E. Zussman [a,*], X. Chen [b], W. Ding [b], L. Calabri [b], D.A. Dikin [b], J.P. Quintana [b], R.S. Ruoff [b,*]

[a] *Department of Mechanical Engineering, Technion—Israel Institute of Technology, Haifa 32000, Israel*
[b] *Department of Mechanical Engineering, Northwestern University, Evanston, IL 60208, USA*

Abstract

The mechanical and structural properties of individual electrospun PAN-derived carbon nanofibers are presented. EELS spectra of the carbonized nanofibers shows the C atoms to be partitioned into ~80% sp^2 bonds and ~20% sp^3 bonds which agrees with the observed structural disorder in the fibers. TEM images show a skin-core structure for the fiber cross-section. The skin region contains layered planes oriented predominantly parallel to the surface, but there are some crystallites in the skin region misoriented with respect to the fiber long axis. Microcombustion analysis showed 89.5% carbon, 3.9% nitrogen, 3.08% oxygen and 0.33% hydrogen. Mechanical testing was performed on individual carbonized nanofibers a few microns in length and hundreds of nanometers in diameter. The bending modulus was measured by a mechanical resonance method and the average modulus was 63 GPa. The measured fracture strengths were analyzed using a Weibull statistical distribution. The Weibull fracture stress fit to this statistical distribution was 0.64 GPa with a failure probability of 63%.
© 2005 Elsevier Ltd. All rights reserved.

Keywords: Carbon nanofibers; Microstructure; Mechanical properties

1. Introduction

Carbon nanofibers, like other quasi-one-dimensional nanostructures such as nanowires and nanotubes, have recently been receiving increased attention. This is due to their potential application as heat-management materials, for composite reinforcement, high-temperature catalysis, membrane-based separation, and as components for nanoelectronics and photonics [1–3].

Carbon fibers are typically produced either by pyrolyzing fibers spun from an organic precursor (e.g., polyacrylonitrile (PAN), or alternatively pitch), or by chemical vapor deposition (CVD) [4]. The spinning method can only produce microscale carbon fibers (diameter >5 μm). CVD can synthesize carbon fibers with diameters ranging from several microns down to 10 nm [5,6].

Recently, carbon fibers were produced by pyrolyzing electrospun nanofibers from PAN [7–9] and from pitch [10] with typical diameters of few hundreds of nanometer and several microns, respectively. However, the structure and the mechanical properties of carbon nanofibers produced from an electropsun polymer precursor are largely unknown. The purpose of this paper is to characterize the structure and to explore the modulus and strength of electropsun PAN-derived carbon nanofibers.

Fibers can be electrospun from polymer solutions in a fairly cost-effective manner [11,12]. Electrospun fibers undergo huge elongation and thinning with a strain rate of ~1000 s^{-1} and the drawing ratio is often as high as

---

* Corresponding authors.
E-mail addresses: meeyal@tx.technion.ac.il (E. Zussman), r-ruoff@northwestern.edu (R.S. Ruoff).

10^4 [13]. The aspect ratio of the fibers, L/d, is in the range of 1000, with diameters (d) of 10–400 nm and lengths (L) up to several centimeters. Recent observations show that both the molecular orientation and the degree of crystallinity of the electrospun fibers are high [14]. The spatial orientation of the as-spun nanofibers can be controlled with an electrostatic field leading to control of deposition geometry. This has potential application in the fabrication of one-dimensional devices or the reinforcement of composite materials [15,16].

As in other fiber processing techniques, the final properties of the carbon fibers are largely determined by the precursor material, and the conditions used to form the precursor fiber. Post-treatment steps (e.g., stretching and carbonization) merely refine and perfect the as-spun structure. Hence, we speculate that the fundamental *structure* and *orientation* of the fiber are established during the electrospinning process. Therefore, to obtain high performance carbon nanofibers, it is important to understand the processing parameters. Due to the special properties of the electrospun PAN precursor and the typical dimensions of the carbonized nanofiber, high modulus and strength are each worthwhile goals to attempt to achieve. Carbonized microfibers are brittle, which suggests they usually fail under mechanical load at critical flaws [17]. Due to the high L/d ratio of the nanofibers, reinforcement of composite materials would be expected to be effective based on the Halpin–Tsai model [18].

This paper initially presents characterization of the structure and chemical composition of the as-spun and then carbonized nanofibers. The investigation of the bending modulus and stress failure of individual carbonized nanofibers is then presented.

2. Experimental procedure

All reagents were used without further purification. Polyacrylonitrile (PAN) with an average molecular weight of $M_w = 150,000$ g/mol (Aldrich) was dissolved in slightly heated *N,N*-dimethylformamide (DMF) to yield an 8 wt.% solution. The polymer solution was electrospun from a 5 ml syringe with a hypodermic needle with an inner diameter of 0.1 mm. A pressure of 150 mbar of air was applied to the solution to control the flow rate. A copper electrode was placed in the polymer solution and the extruded solution was spun onto the sharp edge of a grounded collector disk (for additional details, see Theron et al. [15]). The strength of the electrostatic field was maintained at 0.9 kV/cm and the linear speed of the edge of the disk collector was $V = 5$ m/s. All the experiments were performed at room temperature in air. The as-spun PAN fibers were collected on aluminum oxide (alumina) substrates that were attached on the edge of the collecting wheel. For carbonization, the substrates were placed in a tube furnace and

stabilized in air for 30 min at 250 °C, then carbonized for 1 h in nitrogen at 750 °C, and finally heated at 1100 °C in nitrogen for another hour; the ramp rate was 5 °C/min between the 250, 750, and 1100 °C plateaus.

Raman spectra of the carbon fibers were taken with a Renishaw Raman microspectrometer (514.5 nm excitation, ~15 mW power; ~0.8 μm diameter focus spot using a 100× microscope objective, and a notch filter between 500 and 4000 cm^{-1}). Elemental analysis of the carbonized fibers was performed by microcombustion to detect any traces of carbon, hydrogen and nitrogen, and by pyrolysis to find traces of oxygen. The analysis was performed on a mat of heat-treated nanofibers to within an error of 0.3 wt.% (Atlantic Microlab, Inc.). The fibers were observed under a scanning electron microscope (SEM, LEO Gemini 1525) using an acceleration voltage of 3 kV. The fibers were also observed under a transmission electron microscope (TEM, Hitachi HF-3010). Electron energy loss spectrometry (EELS) was performed in a TEM (Hitachi HF-2000 FEG) to determine the sp^2/sp^3 ratio. A graphite sample (HOPG; ZYB grade, SPI-2, SPI Inc.) served as a reference for pure sp^2 bonding. For the TEM analyses, the fiber deposits were on a SiO TEM grid (Ted Pella, 300 mesh).

The structure of the nanofibers was also examined by wide-angle X-ray diffraction (WAXD) using the DND-CAT at the Synchrotron Research Center at the Advanced Photon Source (14,586.4 eV) at Argonne National Laboratory. The wavelength was $\lambda = 0.85986$ Å. Two-dimensional WAXD patterns were collected using a CCD detector with a spatial resolution of 73.242×73.242 μm. The exposure time for each experiment was 100 s. Calibration was performed using the NIST 674a Titanium oxide (Rutile) and corrundum (Alumina) samples. The nominal sample-to-detector distance was 120 mm. Patterns were obtained from bundles of aligned nanofibers which had been mounted perpendicular to the X-ray beam.

To perform failure testing, a single carbonized fiber was mounted on one end to an AFM cantilever tip (that served as a force-sensing element) and on the other end was glued to the etched tip of a tungsten wire. The setup of the clamped carbonized fiber is shown in Fig. 1. Handling of the fiber and gluing onto the W wire tip were achieved using an optical microscope (Zeiss Axiovert 100; 500× magnification) equipped with mechanical translators. The glue, Hysol® with a shear stress of 20 MPa, was purchased from Dexter Co. The free end of the fiber was clamped onto the tip of the AFM cantilever using electron beam-induced deposition (EBID) [19]. The AFM cantilever, which was purchased from Mikromasch, Inc. (NSC12), had a measured spring constant of $k = 0.47 \pm 0.003$ N/m and was calibrated according to the methods presented by Sader et al. [20] and Dikin et al. [21]. Both the W wire with the attached nanofiber and the AFM cantilever were mounted on a
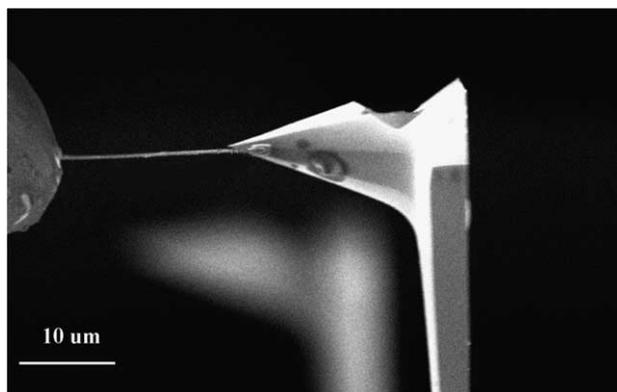
Fig. 1. SEM image of a carbonized nanofiber clamped between an AFM tip and a tungsten wire. A smaller AFM cantilever on the same AFM chip is present in the background.

nano-manipulator [22] which was fixed inside the SEM chamber. Tensile tests of the carbonized fibers were conducted inside the SEM vacuum chamber whereby the applied force was calculated from the observed deflection of the AFM cantilever.

The bending modulus of the carbonized fibers was determined using the natural resonance vibration method [23]. The fiber was bonded to the tip of an AFM cantilever using EBID; the cantilever was itself attached to a piezoelectric bimorph actuator. By applying an alternating electric potential to this piezoactuator, the attached fiber could be driven into mechanical resonance. The SEM chamber pressure was $\sim 10^{-6}$ Torr. The resonance frequency was always much larger than the SEM raster scanning rate so the amplitude of vibration was measured. For a uniform circular cross-section cantilever beam with a free end, the modulus–frequency relationship from the classical analysis of linear elasticity is [24],

$$f_n = \frac{\beta_n^2}{2\pi} \frac{d}{L^2} \sqrt{\frac{E}{16\rho}} \qquad (1)$$

where β_n is the eigenvalue obtained from the characteristic equation $\cosh(\beta_n)\cos(\beta_n) = -1$. For the fundamental mode of vibration, which corresponds to the first eigenvalue, the coefficient $\beta_n = 1.875$. The parameter d is the diameter, L is the length of the nanofiber, and ρ is the material density. E is the Young's modulus, however due to the measurement method we refer to this constant as the *effective bending modulus*. Higher modes were not observed due to vibration power constraints. It was assumed that the resonance frequency was that of the fundamental mode.

3. Results and discussion

3.1. Materials and structural characterization

Fig. 2 shows SEM micrographs of electrospun polymer, and carbonized, nanofibers at different magnifications. After a collection time of 1 h electrospun polymer fibers form a dense mat with a porosity of $\sim 30\%$ and a thickness of 50 μm as shown in Fig. 2a and b. Individual fibers, Fig. 2b, have a uniform cross-section with an average diameter of 220 ± 60 nm, although in some cases beads appear; these are due to capillary instability [25]. In certain instances, a connection between the collected fibers is observed which probably formed during the process of fiber deposition. After the carbonization process (Fig. 2c and d), the mat retained its shape and the average diameter shrank to 110 ± 40 nm.
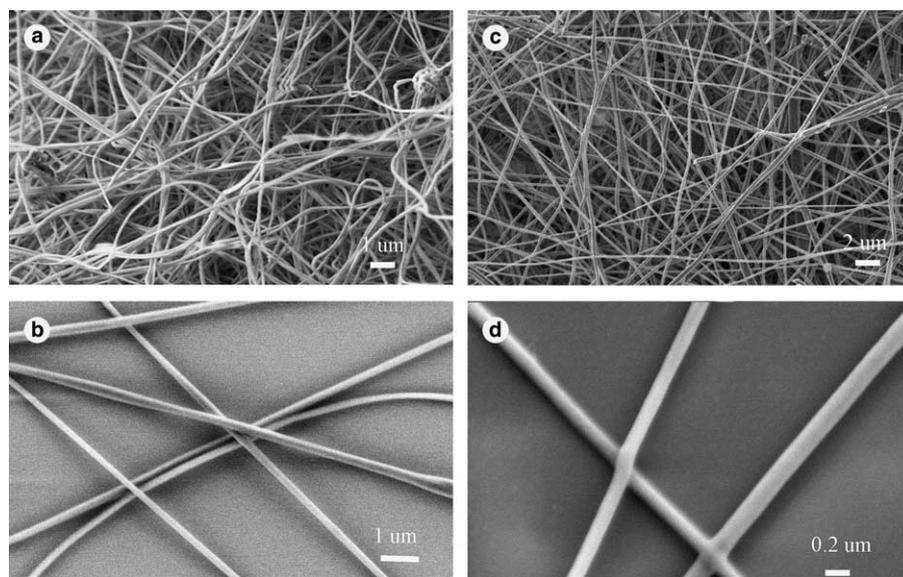

Fig. 2. (a) and (b) Show SEM images of electrospun nanofibers and (c) and (d) show SEM images of carbonized nanofibers, at different magnifications.

Microcombustion and pyrolysis of the carbonized mat showed that the carbonized nanofibers contained 89.47% carbon, some nitrogen (3.93%) and oxygen (3.08%), and a small amount of hydrogen (0.33%). The presence of nitrogen is apparently due to the C–N bonds which are typically found in PAN carbon fibers when the final temperature in the heat treatment is less than 2000 °C [26,27].

Fig. 3 shows the X-ray diffraction pattern of a bundle of electrospun nanofibers. The nanofibers exhibited two equatorial peaks with a diffuse meridian peak. The primary equatorial $(10\bar{1}0)$ peak at $2\theta = 16.88°$ corresponds to a spacing of $d = 5.25$ Å while the weaker reflection $(11\bar{2}0)$ at $2\theta = 29.5°$ corresponds to a spacing of $d = 3.05$Å (note Miller indices $(hkil)$ are used for identification of planes in hexagonal crystals).

The ratio of the d-spacing of these two peaks (1.72) is very close to $\sqrt{3}$:1, indicating hexagonal packing of the rod-like PAN chains [28,29]. The diameter of the chain is approximately $d_{(100)}(2/\sqrt{3}) = 6.06$ Å. Meridional and off-axis scattering is present as a weak, diffuse scattering centered about $2\theta = 38.52°$, corresponding to a spacing of $d = 2.46$ Å which may indicate minor regularity along the chains. Equatorial peaks are commonly observed with PAN fibers, however the scattering at about $2\theta = 38.52°$ is uncommon [28,30,31]. The coherence length, L_c, was determined by analyzing the primary equatorial peak using the Scherrer equation $L_c = \lambda/(B\cos\theta)$, where λ is the wavelength of the X-rays, and B is the width at the half-intensity for the equatorial peaks. The value of the nanofiber crystal size was 53.14 Å. As a reference, the value for a highly oriented fiber containing co-polymer (85% acrylonitrile) was 145 Å [31]. From the X-ray diffraction of the electrospun fibers, the Herman's orientation factor ($f = [3\langle\cos^2\phi\rangle - 1]/2$) for the (100) plane was calculated to be

0.34 ± 0.03. Compared to the Herman's orientation factor of 0.6 for highly oriented melt-spun co-polymer fibers (85% acrylonitrile) [31], and 0.66 for wet-spun co-polymer fibers (90% acrylonitrile) [32], the electrospun PAN shows somewhat lower orientation. However, as-spun fibers undergo post-drawing processes including annealing by heating and cooling under tension, to yield a high level of orientation.

Fig. 4 shows the X-ray diffraction pattern of a bundle of carbonized nanofibers. The bundle exhibits four diffuse equatorial peaks that indicate rather poor orientation: the primary equatorial (002) peak at $2\theta = 24.1°$ (corresponding to a spacing of $d = 3.68$ Å), a weaker reflection (101) (which may overlap the reflection of (100)) at $2\theta = 42.5°$ a diffuse peak of (004) at $2\theta = 52.5°$ and a weak peak of (110) at $2\theta = 77.5°$ The c-axis spacing (d_{002}) is larger than the single crystal value of graphite (0.335 nm for HOPG), which is probably attributable to the presence of H, O, and N, and the presence of sp^3 bonds [26]. The value of the nanofiber crystal size (002) was $L_c = 12.84$ Å. This coherence length is similar to the $L_c = 18.3$ Å measured by Kaburagi et al. [33], for a commercial carbon fiber with a similar amount of C, H and N and with a similar heat treatment (stabilization at 260 °C and carbonization at 1200 °C). Measurements of the scattering at normal incidence, 22.5°, and 45° relative to the X-ray beam, revealed that the sample was isotropic in nature.

Fig. 5 shows a typical Raman spectrum (1100–2000 cm^{-1}) of a bundle of carbonized fibers. There are two broad overlapping peaks centered around 1359.40 cm^{-1} (width 180.01 cm^{-1}) and 1588.60 cm^{-1} (width 119.91 cm^{-1}). These D and G peaks were fitted using a Gaussian–Lorentzian mixed shape [34,35]. The ratio of the integrated intensity of the D and G peaks, $R = I_D/I_G = 0.925 \pm 0.04$, characterizes the disorder in
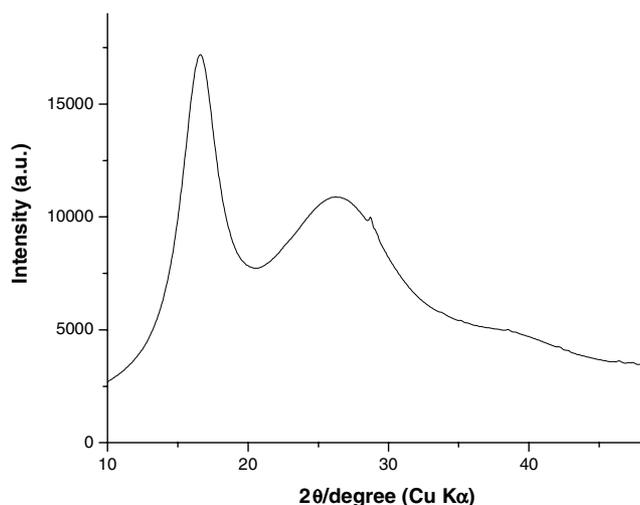

Fig. 3. X-ray diffraction pattern recorded from a bundle of electrospun fibers.
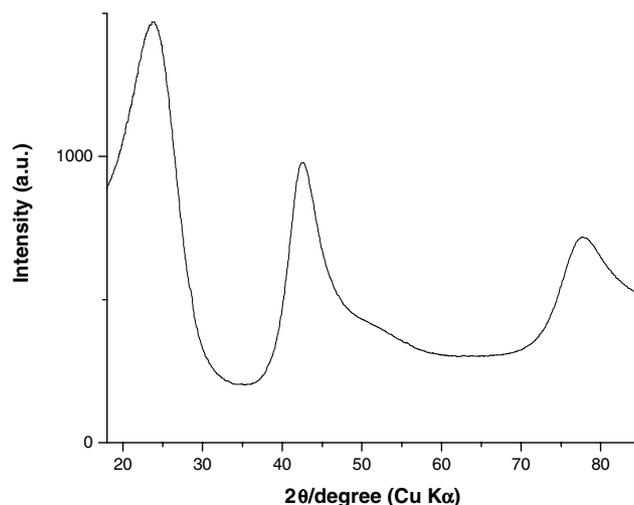

Fig. 4. X-ray diffraction pattern recorded from a bundle of carbonized electrospun fibers.
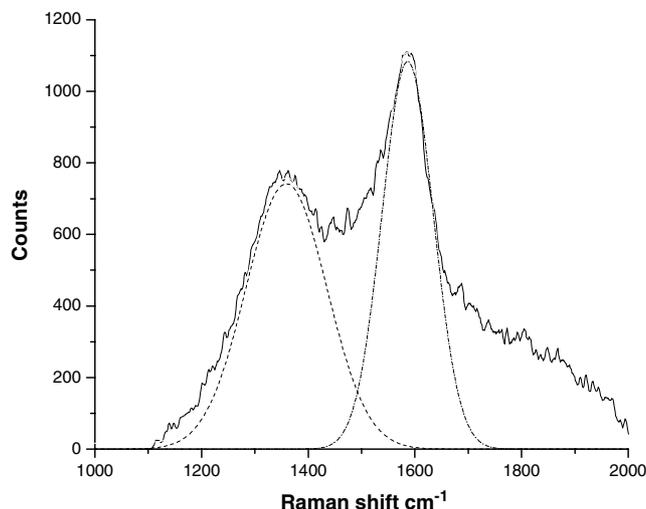
Fig. 5. Raman spectrum of the carbonized PAN nanofibers. The solid line is the spectrum and the dashed line is the superposition of the two fitted Gaussian–Lorentzian peaks.

Fig. 6. EELS spectra of a carbonized fiber mat, and of graphite (HOPG) used as a reference.

the carbon fiber and is a measure of the number of disordered (D), and ordered (G) C atoms [34]. These results are comparable to the Raman spectra of commercial PAN fibers presented by Melanitiis et al. [36] that had undergone heat treatment at 1350 °C. However, the intensity ratio, R, of fibers that were carbonized at higher temperature (>2000 °C), was lower ($R < 0.5$), which is apparently indicative of more highly ordered fibers. Huang and Young [37], however, found that the intensity ratio, R, varies throughout the fiber cross-section; for a commercial PAN fiber (7.8 μm diameter), R varies from 1.5 in the core to 0.5 on the skin, hence variation of the crystal size and orientation across the fiber is demonstrated. Due to the large size of the diameter focus spot of the Raman spectrometer in our setup relative to the typical diameter of the electrospun PAN-derived carbon fiber, we could not distinguish between the skin and the core of the fibers.

EELS was used to further characterize the carbon fibers. Typical EELS spectra acquired from a carbonized PAN fiber in the energy loss range of 280–310 eV are shown in Fig. 6. To determine the fraction of sp^2 and sp^3 carbon bonds, EELS spectra were analyzed by the method proposed by Cuomo et al. [38]. The fraction of the sp^2-bonded C (thus sp^2 bonds divided by the sum of sp^2 and sp^3 bonds) was found to be 0.78 ± 0.05. The confirmed presence of sp^3 bonds is consistent with the presence of the D line in the Raman spectrum, which corroborates the structural disorder expected for this fraction of sp^3 bonds [17].

The transverse structure of carbonized fibers observed by HR-SEM are shown in Fig. 7. The micrographs of fibers that broke during sonication in ultrasonic cleaning baths demonstrate the structural heterogeneity that exists in the cross-section of the fibers. It
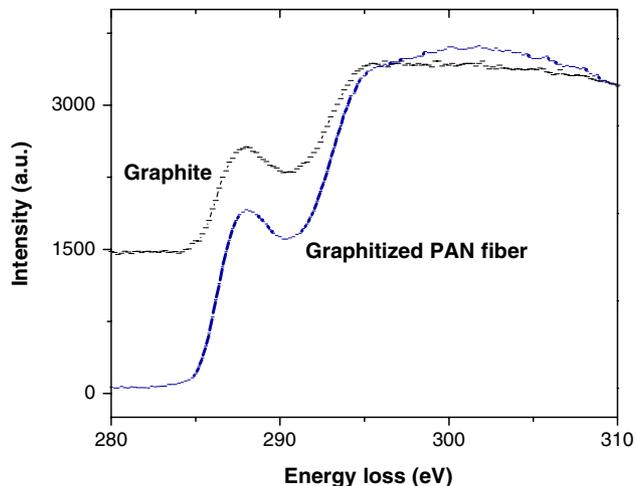
can be seen that the crystalline sheets are oriented radially in the skin and form a tubular structure, but form a random granular-like structure in the core. The thickness of the shell is approximately 10 nm. TEM micrographs of carbonized nanofibers are shown in Fig. 8. A clear aggregation of elongated crystals parallel to the fiber axis is shown. These may be viewed as
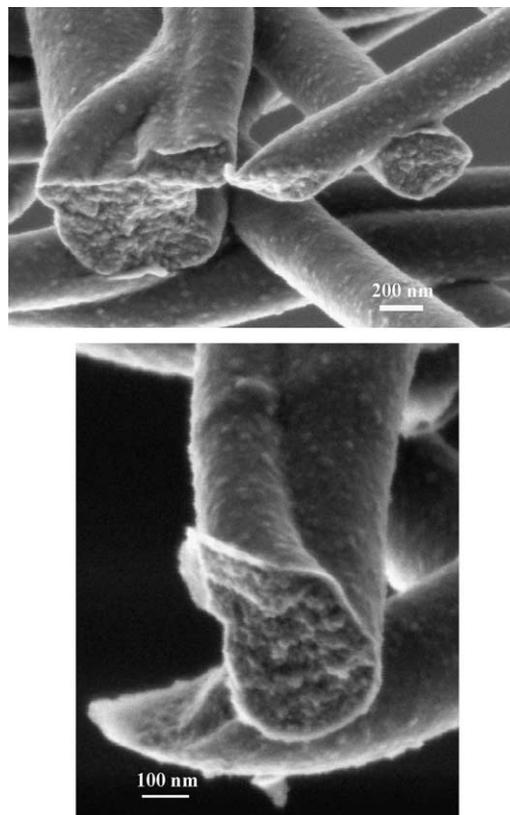

Fig. 7. Two SEM images of the fracture surface of carbonized PAN fibers. The fibers were broken during sonication in an ultrasonic bath.
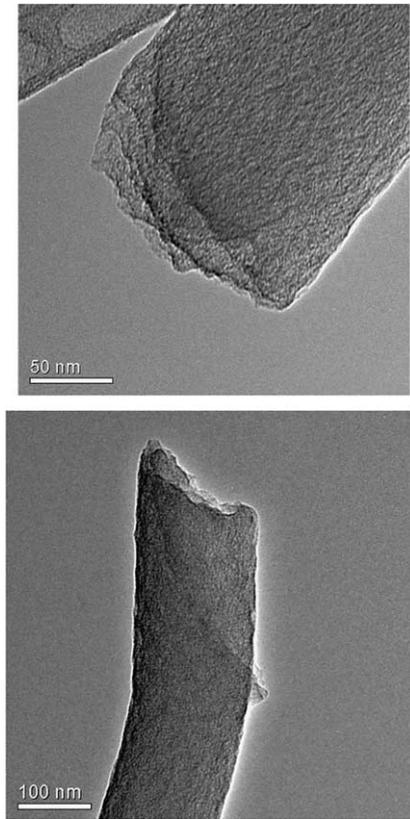
Fig. 8. Two TEM micrographs of the broken edge of carbonized fibers. Several sheath layers can be observed across the edge.

two-dimensional polycrystals with curvilinear anisotropy and a preferred axial direction along the fiber axis. Lattice-fringe images from the longitudinal section of carbonized fibers are shown in Fig. 9. There is evidence of skin-core heterogeneity along the fiber axis. The skin region contains layered planes oriented predominantly parallel to the surface; there are also some crystallites, which can be considered layer plates, which are misoriented with respect to the fiber axis. A similar crystalline configuration was reported by Huang and Young [37] and by Johnson [39] for macroscopic-sized PAN fibers (with a diameter > 5 μm). The micrographs reveal the turbostratic structure: high stacking disorder characteristics, with no regularity of packing in the c-axis [26].

3.2. Mechanical characterization

To derive the bending modulus of the carbon nanofibers, we used the mechanical resonance method. Fig. 10 shows a typical example of a nanofiber driven at its fundamental resonance by the piezoelectric actuator. The quality factor (Q) measured for the nanofibers ranged from 180 to 260. The low Q may reflect the turbostratic structure of the nanofibers. The dependence of the amplitude on frequency (for constant voltage) is approximately Lorentzian, as expected for damped harmonic vibration (see Fig. 11). The fiber in Fig. 11 has a quality factor $Q = 250$ and a bending modulus of $E = 75$ GPa.
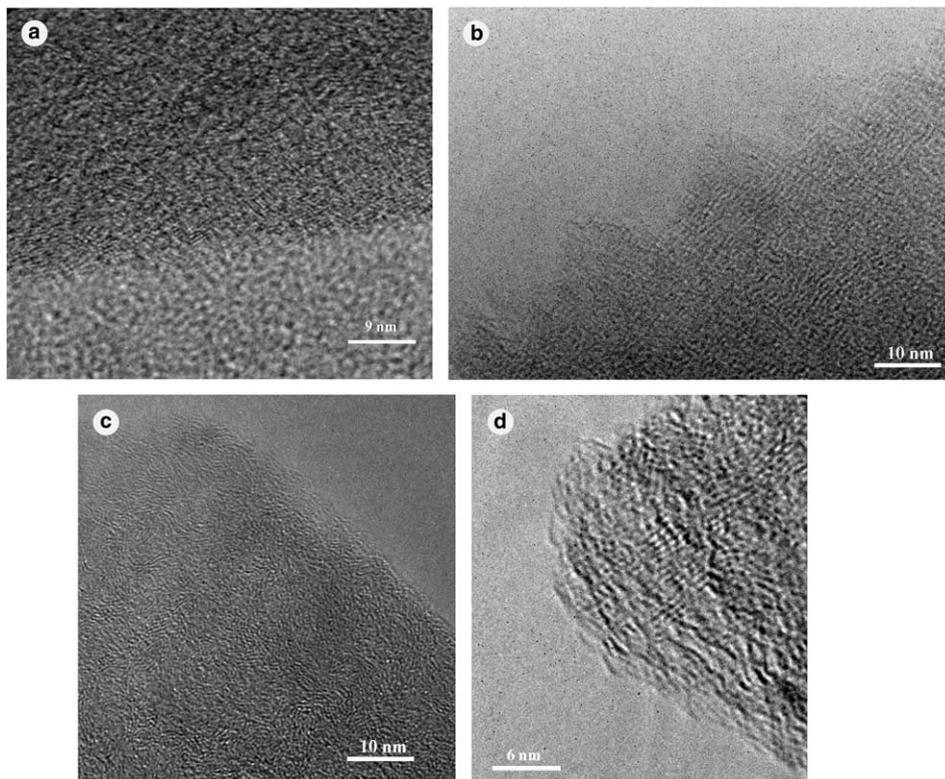

Fig. 9. (a–d) HR-TEM lattice-fringe images from the longitudinal section of carbonized fibers.
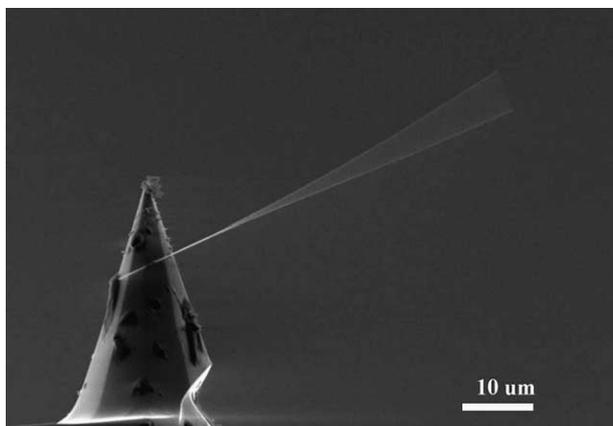
Fig. 10. SEM image of a mechanically resonating nanofiber clamped to an AFM cantilever tip.
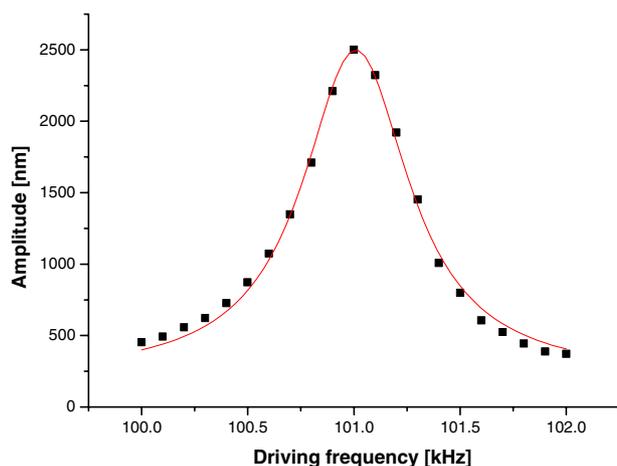

Fig. 11. The amplitude vs. frequency curve for a carbonized fiber mechanically excited at its resonant frequency. The points were fit with a Lorentzian fitting algorithm, and the calculated Q factor is 250.

Lower Qs were observed for fibers that exhibited lower values of the modulus (for example, $Q = 180$, $E = 53$ GPa.) As we did not observe any shift in the resonance frequencies for large amplitude vibrations for any of the measured nanofibers, the response was linear for large amplitude deflections.

Based on the experimentally measured data, the bending modulus of the carbon nanofibers was calculated using Eq. (1). The density of the fibers was assumed to be $\rho = 2.00$ [g/cc]. Some of the experimental results are summarized in Table 1. The average bending modulus of the carbon nanofibers was 63 ± 7 GPa. Since the scale, shape and typical microstructure of the carbon nanofiber were convoluted in the bending modulus measurement, the calculated value cannot be directly compared to the Young's modulus of carbon fibers. As a basis for comparison, the lowest tensile modulus measured for commercial high strength PAN-based carbon fiber was $E = 230$ GPa (ultimate firing temperature 1350 °C) [36].

The failure stress of the carbon fibers varied from 0.32 to 0.90 GPa. For all 19 specimens that were tensile tested, failure occurred in the gauge region. Fig. 12 shows SEM micrographs of the fracture surface of a carbonized PAN fiber. In Fig. 12a–c a fiber with a roughly circular cross-section is shown in different perspective views and at different levels of magnification. The core of the fiber shows a random arrangement, while the skin has a circumferential arrangement. In Fig. 12d and e, the surfaces of carbonized fibers at fracture sites are shown. While the failure was probably due to shear or a combination of stresses, it can also be seen that the cores in these fibers reveal a random arrangement.

Since these carbonized fibers are a brittle material, the lack of ductility or yielding leads to large data scatter in strength testing. That fracture occurs randomly in the gauge region (rather than always occurring close to the clamps, where a stress concentration is present) suggests that there is a distribution of defects in these nanofibers and that at least one critical defect that provides a higher stress concentration than near the clamps may be present for each. The fracture strength of the carbonized fiber is apparently determined by a combination of the microstructure and variable defect size and shape, assuming that the toughness of the fiber is an intrinsic property and does not vary. Since the flaws are randomly distributed, the measured strength could depend on the length and diameter of the fibers—the greater the volume of the fiber, the greater the number of flaws, and the higher the probability of several flaws being present.

It is known that the strength distribution of brittle materials can be described by the Weibull cumulative distribution function. Weibull statistics as they apply

Table 1
Bending modulus of electrospun PAN-derived carbon nanofibers

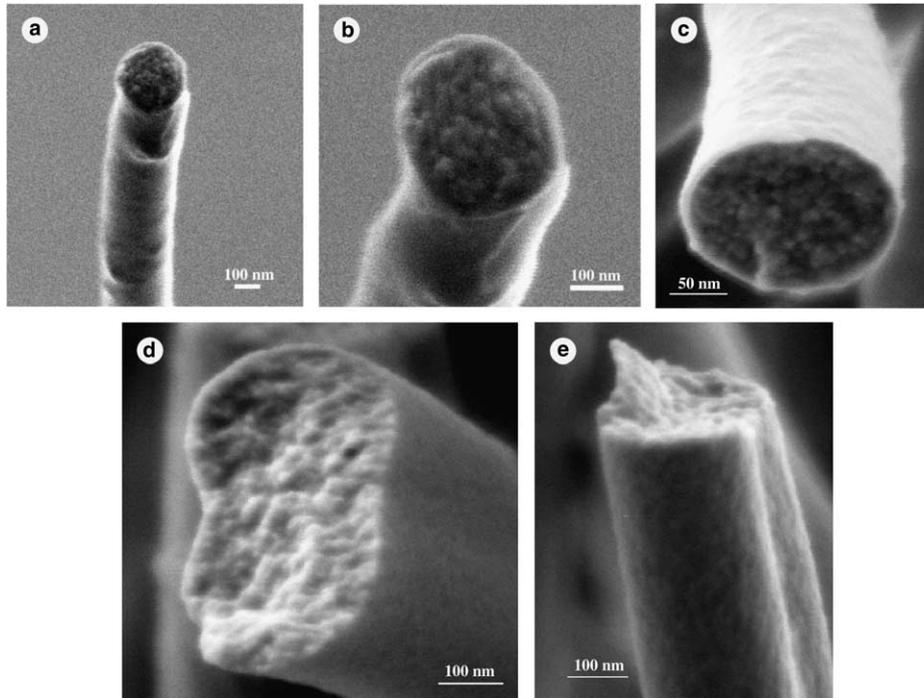| Length [μm] (±0.2)	Diameter [nm] (±5)	Nat. frequency [kHz]	Young's modulus, E [GPa]
17	200	534.6	61.0 (±3.24)
24.3	115	161.0	69.8 (±3.80)
13.8	105	414.0	57.6 (±4.32)
11.51	181	988.7	53.5 (±4.00)
33.61	150	114.0	75.3 (±3.08)
78.27	114	13.98	57.7 (±2.59)

Fig. 12. (a–e) SEM images of fracture surfaces of carbonized fibers after tensile loading to break.

to strength values provide a probability of failure at given stress levels. The Weibull probability function for tensile test structures, assuming that the structure is incompressible, is [40,41]

$$P_{\mathrm{f}} = 1 - \exp\left[-\left(\frac{\sigma_{\mathrm{a}}}{\sigma_0}\right)^m\right] \tag{2}$$

where P_{f}, the failure probability, is a function of σ_{a}, the applied stress, σ_0 is the scaling factor and the exponent m is a material parameter called the 'Weibull modulus'. The failure probability of a specimen can be calculated using the *median ranking* which is recommended for moderate size samples [42]. Thus, σ_0 and m are the unknowns of the Weibull distribution that must be determined experimentally. An assumption of the above Weibull model (Eq. (2)) is that the fibers to be modeled are of the same volume. Of the experimental results presented herein, only the fibers whose volumes were in the same range (1.5–2 μm^3) were used in the Weibull analysis. The results of the failure stress measurements are shown in Fig. 13. Applying the *median rank regression* curve fitting, using the failure stress σ_0 as the dependent variable, resulted in $\sigma_0 = 0.64$ GPa and $m = 3.2$. This indicates that 63%, that is, $(1 - e^{-1}) \cdot 100\%$ of the specimens will fail when the stress reaches σ_0. The goodness of the fit to the straight line in Fig. 13 is $r^2 = 0.92$. For comparison, we apply the *maximum likelihood estimates* (MLE) which resulted in $\sigma_0 = 0.62$ GPa and $m = 3.5$. In this method, the confidence intervals (95%) for the estimates of σ_0 and m were: lower bounds: $\sigma_0 = 0.55$ GPa, $m = 2.5$, and upper bounds: $\sigma_0 = 0.71$ GPa, $m = 5.0$.
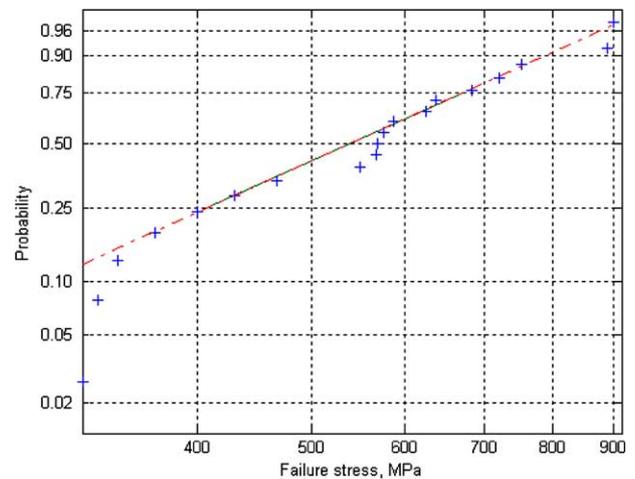

Fig. 13. Weibull probability plot for carbonized fibers ($m = 3.2$, $\sigma_0 = 0.64$ GPa).

As a comparison, the lowest tensile strength that was measured for commercial high strength PAN-based carbon fiber was $\sigma_0 = 1.86$ GPa [37]. Fig. 14 presents the carbon fiber failure stress as a function of the gauge length. It seems that the failure stress of the carbon fibers slightly decreases as the gauge length of the specimen increases. Fig. 15 presents the carbon fiber failure stress as a function of its diameter. As can be seen in the graph, the failure stress is slightly decreased as the surface area of the fiber increases. In both graphs, we believe that due to the 3-D heterogeneous structure of the
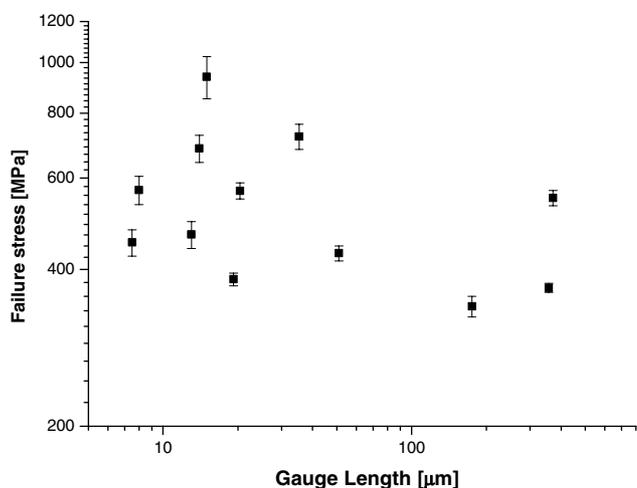
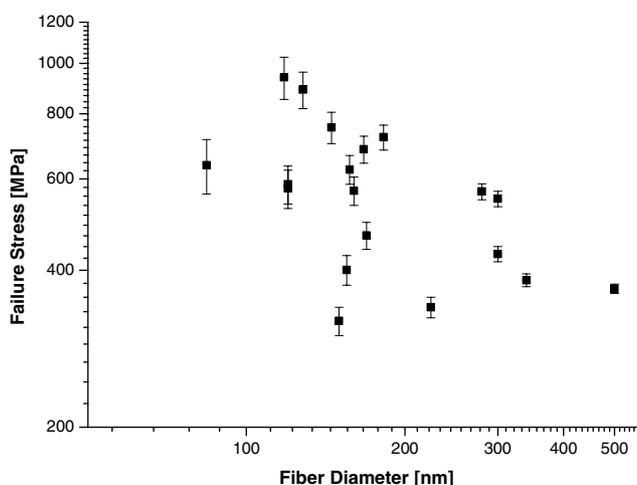Fig. 14. Carbon fiber failure stress as a function of the gauge length.

Fig. 15. Carbon fiber failure stress as a function of the fiber diameter.

carbonized fibers, namely the cross-sectional as well as longitudinal heterogeneity of the fibers, we cannot expect a simple relation between the failure stress and a single parameter such as the length or the diameter [43].

4. Conclusions

In summary, this work describes the fabrication of electrospun PAN-derived carbon nanofibers that were then carbonized, with diameters ranging from 50 to 250 nm. The production of such nanofibers represents an important step for study of their structure and properties, and for further developing them for potential use in composites or as individual elements. A high degree of orientation of the as-spun nanofiber was obtained, which can be explained by the structure formed during the electrospinning process. EELS spectra of the carbonized nanofibers shows the C atoms to be partitioned

into ~80% sp^2 bonds and ~20% sp^3 bonds which agrees with the observed structural disorder in the fibers.

SEM and TEM images show a skin-core structure for the fiber cross-section. The skin region contains layered planes oriented predominantly parallel to the surface, but there are some crystallites in the skin region, hence layered planes, which were misoriented with respect to the fiber long axis. Such a turbostratic structure has been reported previously [26,44,45]. Microcombustion results of a mat carbonized nanofibers showed 89.5% carbon and 3.9% nitrogen, 3.08% oxygen and 0.33% hydrogen.

The bending modulus of individual nanofibers was measured by a mechanical resonance method and the average modulus was 63 GPa. The fracture strength of the carbonized fibers were analyzed using a Weibull statistical distribution based on the assumption that the variation in strength is caused by a variation in the stress concentration from a critical defect in a given volume of material. The Weibull fracture stress fit to this statistical distribution was 0.64 GPa with a failure probability of 63%. The Weibull strength of the material was assessed using a constant specimen volume. Future work should examine the strength of specimens having a range of volumes (i.e., with varying lengths and diameters) in order to fully examine the applicability of the Weibull theory of failure. It is expected that in studying smaller volumes, it will be found that the defect distribution will be highly dependent on the material's microstructure.

Comparing the mechanical properties of the electrospun PAN-derived carbon nanofibers to commercial PAN-derived carbon fibers is of interest. Besides the size effect (the diameter of commercial fibers is greater than 5 μm), the commercial carbonized fibers are usually produced from co-polymers (e.g., 10% methyl methacrylate), subjected to post-drawing processes with heating under tension, and carbonized at between 1400 and 1700 °C [17]. As this is the first paper, to our knowledge, addressing both fabrication and mechanical investigation of electrospun carbon nanofibers, it is perhaps premature to conclude that the mechanical properties of electrospun PAN-based carbon nanofibers will always be inferior to the commercial PAN-based fibers; certainly, the stiffness and strength of those discussed here are lower than commercial PAN-based fibers. If the polymer precursor morphology and molecular orientation, along with the carbonization process, can be optimized it is possible that the stiffness and fracture strength of carbon nanofibers based on the electrospinning process could be substantially improved.

Acknowledgments

References

[1] Lieber CM. The incredible shrinking circuit—Researchers have built nanotransistors and nanowires. Now they just need to find a way to put them all together. Sci Amer 2001;285(3):58–64.

[2] Hammel E, Tang X, Trampert M, Schmitt T, Mauthner K, Eder A, et al. Carbon nanofibers for composite applications. Carbon 2004;42(5–6):1153–8.

[3] Chand S. Carbon fibers for composites. J Mater Sci 2000;35(6):1303–13.

[4] Pierson HO. Handbook of carbon, graphite, diamond and fullerenes. New Jersey: Noyes Publications; 1993.

[5] Endo M, Kim YA, Takeda T, Hong SH, Matusita T, Hayashi T, et al. Structural characterization of carbon nanofibers obtained by hydrocarbon pyrolysis. Carbon 2001;39(13):2003–10.

[6] Zheng GB, Kouda K, Sano H, Uchiyama Y, Shi YF, Quan HJ. A model for the structure and growth of carbon nanofibers synthesized by the CVD method using nickel as a catalyst. Carbon 2004;42(3):635–40.

[7] Chun I, Reneker DH, Fong H, Fang XY, Dietzel J, Tan NB, et al. Carbon nanofibers from polyacrylonitrile and mesophase pitch. J Adv Mater 1999;31(1):36–41.

[8] Ko F, Gogotsi Y, Ali A, Naguib N, Ye HH, Yang GL, et al. Electrospinning of continuous carbon nanotube-filled nanofiber yarns. Adv Mater 2003;15(14):1161–5.

[9] Wang Y, Serrano S, Santiago-Aviles JJ. Raman characterization of carbon nanofibers prepared using electrospinning. Syn Metals 2003;138(3):423–7.

[10] Park SH, Kim C, Yang KS. Preparation of carbonized fiber web from electrospinning of isotropic pitch. Syn Metals 2004; 143(2):175–9.

[11] Huang ZM, Zhang YZ, Kotaki M, Ramakrishna S. A review on polymer nanofibers by electrospinning and their applications in nanocomposites. Compos Sci Technol 2003;63(15):2223–53.

[12] Yarin AL, Zussman E. Upward needleless electrospinning of multiple nanofibers. Polymer 2004;45(9):2977–80.

[13] Reneker DH, Yarin AL, Fong H, Koombhongse S. Bending instability of electrically charged liquid jets of polymer solutions in electrospinning. J Appl Phys 2000;87(9):4531–47.

[14] Dersch R, Liu TQ, Schaper AK, Greiner A, Wendorff JH. Electrospun nanofibers: Internal structure and intrinsic orientation. J Polym Sci Part a—Polym Chem 2003;41(4):545–53.

[15] Theron A, Zussman E, Yarin AL. Electrostatic field-assisted alignment of electrospun nanofibres. Nanotechnology 2001;12(3): 384–90.

[16] Zussman E, Theron A, Yarin AL. Formation of nanofiber crossbars in electrospinning. Appl Phys Lett 2003;82(6):973–5.

[17] Fitzer E. Pan-based carbon-fibers present state and trend of the technology from the viewpoint of possibilities and limits to influence and to control the fiber properties by the process parameters. Carbon 1989;27(5):621–45.

[18] Halpin J, Kardos J. Halpin–Tsai equations—review. Polym Eng Sci 1976;16(5):344–52.

[19] Ding W, Dikin DA, Chen X, Wang X, Li X, Piner RD, et al. Mechanics of hydrogenated amorphous carbon deposits from electron beam induced deposition of a paraffin precursor. J Appl Phys (in press).

[20] Sader JE, Larson I, Mulvaney P, White LR. Method for the calibration of atomic-force microscope cantilevers. Rev Sci Instrum 1995;66(7):3789–98.

[21] Dikin DA, Chen X, Ding W, Wagner G, Ruoff RS. Resonance vibration of amorphous SiO_2 nanowires driven by mechanical or electrical field excitation. J Appl Phys 2003;93(1):226–30.

[22] Yu MF, Dyer MJ, Skidmore GD, Rohrs HW, Lu XK, Ausman KD, et al. Three-dimensional manipulation of carbon nanotubes under a scanning electron microscope. Nanotechnology 1999; 10(3):244–52.

[23] Poncharal P, Wang ZL, Ugarte D, de Heer WA. Electrostatic deflections and electromechanical resonances of carbon nanotubes. Science 1999;283(5407):1513–6.

[24] Timoshenko SP. Theory of elastic stability. 2nd ed. New York: McGraw-Hill; 1961.

[25] Koombhongse S, Liu WX, Reneker DH. Flat polymer ribbons and other shapes by electrospinning. J Polym Sci Part B—Polym Phys 2001;39(21):2598–606.

[26] Dresselhaus MS, Dresselhaus G, Sugihara K, Spain IL, Goldberg HA. Graphite fibers and filaments. Berlin: Springer Verlag; 1988.

[27] Zhang WX, Liu J, Wu G. Evolution of structure and properties of PAN precursors during their conversion to carbon fibers. Carbon 2003;41(14):2805–12.

[28] Allen RA, Ward IM, Bashir Z. The variation of the D-spacings with stress in the hexagonal polymorph of polyacrylonitrile. Polymer 1994;35(19):4035–40.

[29] Liu XD, Ruland W. X-ray studies on the structure of polyacrylonitrile fibers. Macromolecules 1993;26(12):3030–6.

[30] Dalton S, Heatley F, Budd PM. Thermal stabilization of polyacrylonitrile fibres. Polymer 1999;40(20):5531–43.

[31] Davidson JA, Jung HT, Hudson SD, Percec S. Investigation of molecular orientation in melt-spun high acrylonitrile fibers. Polymer 2000;41(9):3357–64.

[32] Sreekumar TV, Liu T, Min BG, Guo H, Kumar S, Hauge RH, et al. Polyacrylonitrile single-walled carbon nanotube composite fibers. Adv Mater 2004;16(1):58.

[33] Kaburagi M, Bin YZ, Zhu D, Xu CY, Matsuo M. Small angle X-ray scattering from voids within fibers during the stabilization and carbonization stages. Carbon 2003;41(5):915–26.

[34] Ferrari AC, Robertson J. Interpretation of Raman spectra of disordered and amorphous carbon. Phys Rev B 2000;61(20): 14095–14107.

[35] Lespade P, Aljishi R, Dresselhaus MS. Model for Raman-scattering from incompletely graphitized carbons. Carbon 1982; 20(5):427–31.

[36] Melanitis N, Tetlow PL, Galiotis C. Characterization of PAN-based carbon fibres with laser Raman spectroscopy. 1. Effect of processing variables on Raman band profiles. J Mater Sci 1996;31(4):851–60.

[37] Huang Y, Young RJ. Effect of fiber microstructure upon the modulus of pan-and pitch-based carbon-fibers. Carbon 1995;33(2):97–107.

[38] Cuomo JJ, Doyle JP, Bruley J, Liu JC. Sputter deposition of dense diamond-like carbon-films at low-temperature. Appl Phys Lett 1991;58(5):466–8.

[39] Johnson DJ. Recent advances in studies of carbon fibre structure. Philos Trans R Soc Lond Ser A, Math Phys Sci 1980;294(1411): 443–9.

[40] Jayatilaka AS. Fracture of engineering brittle materials. Applied Science Publishers; 1979.

[41] Weibull W. A statistical distribution function of wide applicability. J Appl Mech 1951;18:293–7.

[42] Abernethy RB. The new Weibull handbook: Reliability & statistical analysis for predicting life, safety, survivability, risk, cost and warranty claims, 4th ed., Dr. Robert Abernathy, 2000.

[43] Altus E. Analysis of Bernoulli beams with 3D stochastic heterogeneity. Prob Eng Mech 2003;18(4):301–14.

[44] Warren BE. X-ray diffraction in random layer lattices. Phys Rev 1941;59(9):693–8.

[45] Oberlin A, Endo M, Koyama T. Filamentous growth of carbon through benzene decomposition. J Cryst Growth 1976;32(3): 335–49.